Desalination and Water Treatment
www.deswater.com
doi: 10.5004/dwt.2022.28540

261 (2022) 241–248
June

Removal of Se(IV) from water with biochar-supported nanoscale zero-valent iron: optimization of preparation conditions and adsorption characteristics

Meijing Chen[a,b], Wenfeng Liu[c], Baojun Yi[a,b,*], Yunlian Wu[a], Xiangdong Kong[a], Shiwei Zhang[a], Zhengshuai Sun[a]

[a]*College of Engineering, Huazhong Agricultural University, No. 1, Shizishan Street, Hongshan District, Wuhan 430070, China, Tel./Fax: +86 27 87282120; emails: bjyi@mail.hzau.edu.cn (B. Yi), 2017307220432@webmail.hzau.edu.cn (M. Chen), 18715453336@163.com (Y. Wu), lemon2021@webmail.hzau.edu.cn (X. Kong), zhangshiwei@webmail.hzau.edu.cn (S. Zhang), 2019307110037@webmail.hzau.edu.cn (Z. Sun)*
[b]*Key Laboratory of Agricultural Equipment in the Mid-lower Yangtze River, Ministry of Agriculture, Wuhan 430070, China*
[c]*China Tobacco Hubei Industrial Co., Ltd., Wuhan 430052, China, email: lwf8237@163.com (W. Liu)*

Received 31 December 2021; Accepted 22 April 2022

ABSTRACT

Se(IV) in wastewater is a problem due to its high solubility, mobility, and potential toxicity. The purpose of this study was to develop biochar-supported nanoscale zero-valent iron (BC-nZVI), investigate the preparation conditions and adsorption properties, and explore the removal mechanism of Se(IV). The results illustrated that the adsorption capacity of Se(IV) increased with an increase of pyrolysis temperature. As pyrolysis time rose, the adsorption capacity was increased at low temperature (300°C). Nevertheless, it first increased and then decreased at higher temperatures (400°C and 600°C). The ratio of raw materials also affected the removal of Se(IV). NaOH modification enhanced the adsorption capacity. The –OH had a great influence on the adsorption of Se(IV). With the increase of initial pH, the adsorption capacity increased first and then decreased. The adsorption of Se(IV) fits the pseudo-first-order and pseudo-second-order models, indicating that the adsorption behavior of Se(IV) by BC-nZVI was determined by both physical and chemical mechanisms, of which physical adsorption dominated. The consequence made clear that BC-nZVI synthesized in this experiment had advantages of a simple process and excellent performance. It is a promising material for removing Se(IV) from water.

Keywords: Biochar; Adsorption; Selenite; Nanoscale zero-valent iron (nZVI); Wastewater treatment

1. Introduction

At present, coal-fired power plants account for more than 50% of the total global selenium emissions. The selenium content in Chinese coal is higher than the world average, and the energy structure is dominated by coal burning, which leads to severe selenium pollution in the environment. Selenium exists in several diverse valence states, of which selenate (Se(VI)) and selenite (Se(IV)) have high solubility, mobility, and potential toxicity in the water environment [1], and Se(IV) is almost 10 times more toxic than Se(VI). The wet limestone-gypsum desulfurization process is a widely adopted flue gas treatment method, and the selenium concentration in the treated wastewater is 1–10 mg/L. However, in China, the maximum allowable limit of selenium in wastewater is 0.5 mg/L, so it is urgent

* Corresponding author.

to develop a feasible sewage treatment method to remove Se(IV) from water.

There are many methods for removing Se(IV) from wastewater, including adsorption, membrane separation, ion exchange, flocculation precipitation, and chemical reduction, etc. The adsorption method is widely used on account of its simple operation, low cost, and effective removal. In recent years, zero-valent iron (ZVI) has been valued in water environment remediation because of its superiorities of hypotoxicity, low cost, and less secondary pollution, which can remove Se(IV) from water not only by adsorption but also via reduction reaction and co-precipitation [2]. Therefore, it is typically used as an effective material to remove Se(IV) from wastewater.

Nanoscale zero-valent iron (nZVI) possesses higher surface activity and specific surface area than ZVI; hence, it is more effective in wastewater treatment. Wang et al. [3]. found that the removal capacity by nZVI on heavy metal (Ag^+ and AsV) was negatively correlated with the particle size, and the smaller the volume, the more active the chemical reaction. Nevertheless, nZVI has defects as well. It tends to agglomerate, resulting in limited migration capacity and reduced specific surface area and reactivity [4], and the rate of aggregation rises with the increase of particle concentration. When the initial concentration was 60 mg/L, the cluster size reached 20–70 μm within 30 min and precipitated rapidly from solution [5]. At the same time, it is easy to passivate [6]. When nZVI participated in the reaction alone, the pollutant ions and Fe(III) generated by redox reaction accumulated and precipitated on its surface, making the life of nZVI shorter [7]. Furthermore, nZVI particle size is too small, which frequently appears in the form of powder, and when directly used in water treatment, it brings about iron pollution [8].

Diverse techniques have been explored to improve the stability of nZVI to deal with these problems. Previous studies have found that fixing nZVI on the support material is an effective method, which not only makes nZVI more dispersed and stable but retains the characteristics of the two materials. A variety of materials have been used to fix nZVI, such as clay, graphene, activated carbon, and biochar (BC). Among them, clay has favorable ion exchange capacity and large specific surface area, but there is insufficient capacity to produce active substances, and it's difficult to separate and recycle. Graphene and other novel carbon-based materials may be at risk of polluting the environment, efficient separation and recovery is also the key to its technology. Activated carbon has similar properties to BC, but it is more expensive. Choosing BC as support material has remarkable advantages: (i) low cost, (ii) it effectively addresses the problem of agricultural waste disposal in China and is environmentally friendly, (iii) it is a widely used adsorbent in of itself. In preceding studies, biochar-supported nanoscale zero-valent iron (BC-nZVI) has been utilized to remove multiple pollutants. Wang et al. [9] reported that pine wood biochar-supported with nZVI has a certain removal ability of arsenate (As(V)), and Wu et al. [10] reported that BC-nZVI can effectively remove Cr(VI) in wastewater. Li et al. [11] studied the synthesis and characterization of nZVI-HPB and application for lead ion removal.

Tan et al. [12] studied the influence factors of Se(IV) removal from water by BC-nZVI. Previous studies demonstrated that pyrolysis temperature and time dramatically impacted the physiochemical properties of BC, and further affected the distribution and particle size of nZVI [13]. In addition, the suitable ratio of BC to nZVI enables the distribution of nZVI more uniform, thus providing more active sites for pollutants. Because different chemical modifications may alter the specific surface area, charge, and surface functional groups of BC, etc., there is a certain impact on the removal ability of pollutants by BC-nZVI as well [7]. Moreover, few studies have reported on the adsorption characteristics and kinetic mechanism of Se(IV) removal in water by BC-nZVI.

In this study, BC was prepared from rice straw, and then BC-nZVI was successfully synthesized by reducing Fe^{2+} with $NaBH_4$. The effects of pyrolysis conditions, raw material ratio, and chemical modification on Se(IV) removal were studied, and the Se(IV) removal performance by BC-nZVI was tested under different adsorbent dosage and solution pH. Experimental conditions for removing Se(IV) were optimized, and the kinetics of the adsorption process was investigated, which provide theoretical support for the application of BC-nZVI in removing Se(IV) from water.

2. Experimental

2.1. Materials

Rice straw was gathered in Suqian, Jiangsu, washed with deionized water, dried, smashed, and passed through 60- to 200-mesh sieves. $FeSO_4·7H_2O$, $NaBH_4$, Na_2SeO_3, C_2H_5OH, NaOH, HCl, H_2O_2, and KBr were purchased from Sinopharm Chemical Reagent Co., Ltd., (Shanghai, China). All reagents were analytically pure. Solutions were prepared with ultrapure water.

2.2. Preparation of BC

A quartz boat containing a certain amount of smashed rice straw was inserted into the pre-heated electric tube furnace (Beijing Yongguangming Medical Instrument Co., Ltd., Beijing, China) and passed through N_2 flow to create an oxygen-free environment. The pyrolysis was completed after heating at target temperatures (300°C, 400°C, and 600°C) for a period of time (30, 60, 90, and 120 min). The obtained biochar was cooled to normal temperature in an N_2 atmosphere, stored in plastic bags after washing and drying, and labeled as BC. In addition, BC pyrolysis under 600°C with 30 min was chemically modified with 1 mol/L HCl, 1 mol/L NaOH, and 30% H_2O_2, respectively. To be specific, BC was soaked in the condition of the mass ratio of solid to liquid was 1:50 for 24 h, then washed and dried, and labeled as BC_{600}-HCl, BC_{600}-NaOH, and BC_{600}-H_2O_2, respectively.

2.3. Preparation of BC-nZVI

In this experiment, BC-nZVI was prepared using a liquid-phase reduction method. Substances were added to the conical flask in the order of $FeSO_4·7H_2O$, ultrapure

water, BC, and C_2H_5OH (N_2 was passed through the overall preparation process to eliminate interference), and the suspension was stirred for 1 h (200 rpm). Afterwards, 50 mL $NaBH_4$ solutions (20 g/L) were slowly dropped into the mixed solution, in which Fe^{2+} was subjected to a reduction reaction according to Eq. (1) [14]. After 1 h of reaction, the resultant BC-nZVI was alternately washed with C_2H_5OH and ultrapure water, dried and stored in plastic bags, and labeled as BC-nZVI. Furthermore, BC-nZVI prepared with BC-HCl, BC-NaOH, and BC-H_2O_2 as supports were marked as BC-HCl-nZVI, BC-NaOH-nZVI and BC-H_2O_2-nZVI, respectively. The molar ratios of BC to nZVI (BC-nZVI) were 1, 2, 4, and 6 (the mass of $FeSO_4{\cdot}7H_2O$ was 2.482 g and the mass of BC was 0.5, 1.0, 2.0, and 3.0 g, respectively). The volume ratios of C_2H_5OH to ultrapure water (ET/H_2O) were 0.5, 1, 2, and 4 (the volumes of C_2H_5OH and ultrapure water were 50, 100, 75, 75, 100, 50, 120, and 30 mL , respectively).

$$2Fe^{2+} + BH_4^- + 2H_2O = 2Fe^0 + BO_2^- + 2H_2 + 4H^+ \quad (1)$$

2.4. Fourier-transform infrared spectroscopy

Samples to be tested and KBr powders were mixed uniformly under the condition of the mass ratio of KBr to the sample being 150:1, and a Fourier transform infrared spectrometer (Thermo Fisher Scientific, Shanghai, China) was utilized to investigate surface functional groups of adsorbents between 400 and 4,000 cm^{-1}.

2.5. Batch adsorption experiments

To explore the effect of adsorbent dosage on adsorption experiment, diverse dosages (0.25, 0.5, 0.75, 1, and 2 g/L) of BC-nZVI were added to the plastic bottle containing 10 mg/L Se(IV) solution (50 mL, pH 7 (neutral pH)). Residual Se(IV) in the solution was measured after shaking under the condition of 300 rpm and 25°C for 2 h. The pH of Se(IV) solution was adjusted between 3 and 10 with 0.1 M HCl solution and 0.1 M NaOH solution, and 1 g/L of BC-nZVI was added to the plastic bottle containing 10 mg/L Se(IV) solution (50 mL) for batch adsorption to investigate the effect of initial solution pH on Se(IV) removal. The adsorption kinetics used 10 mg/L Se(IV) solution (50 mL, pH 7) and 1 g/L BC-nZVI, and the supernatant was extracted at 10, 20, 30, 60, 90, and 120 min, respectively. A blank control sample (without adsorbents) was prepared for each batch of adsorption experiments to decrease the interference of other factors. All experiments were performed in triplicate.

2.6. Analysis

The adsorption capacity q_t (mg/g) and removal rate Re (%) at time t are shown in the following formulae:

$$q_t = \frac{\left[\left(C_0 - C_t\right) \times V\right]}{M} \quad (2)$$

$$\mathrm{Re} = \left[\frac{\left(C_0 - C_e\right)}{C_0}\right] \times 100\% \quad (3)$$

where C_0 (mg/L), C_t (mg/L), and C_e (mg/L) represent the initial concentration, the concentration at time t (min) and the concentration when reaching adsorption equilibrium, respectively, and V (L) and W (g) represent the volume of solutions and the mass of adsorbents added, respectively.

Dynamic models were used to fit the experimental data [15] as follows:

$$q_t = q_e\left[1 - \exp\left(-K_1 \times t\right)\right] \quad (4)$$

$$q_t = \frac{K_2 \times q_e^2 \times t}{\left(1 + K_2 \times q_e \times t\right)} \quad (5)$$

$$q_t = K_p \times t^{0.5} + C \quad (6)$$

where q_e is the adsorption capacity at adsorption equilibrium time (mg/g), q_t is the adsorption capacity (mg/g) at the time of t (min), K_1 is the rate constant of pseudo-first-order, K_2 is the rate constant of pseudo-second-order, K_p is the rate constant of intraparticle diffusion (mg $min^{0.5}$/g), and C is a constant (mg/g).

3. Results and discussion

3.1. Effect of preparation conditions on the removal of Se(IV)

The BC possessed diverse specific surface regions when prepared at various pyrolysis temperature and time [16], which led to different removal capacity of BC-nZVI, as shown in Fig. 1. With increased pyrolysis temperature, the adsorption capacity of Se(IV) increased on account of the larger specific surface area and total pore volume of BC prepared under high-temperature conditions [17], bringing about an increase in the active sites of nZVI, and thereby an enhancement in the Se(IV) removal capacity. As pyrolysis time rose, the adsorption capacity of Se(IV) gradually increased. On the contrary, after more than 90 min, the removal capacity of BC-nZVI generated at higher temperatures (400°C and 600°C) diminished. Under high-temperature conditions, with pyrolysis time growing, gasification reaction occurred on some carbon surfaces, and the rich pore structure generated by the release of volatilization in the early stage collapsed [18], resulting in a reduction in BC surface area and thus a decrease in nZVI active sites. The pyrolysis temperature and time when reaching the maximum adsorption capacity were 600°C and 90 min, respectively, so they were selected as the optimum preparation condition to carry out subsequent adsorption experiments.

As shown in Fig. 2, the removal capacity of Se(IV) was enhanced gradually with the increase of pyrolysis temperature. Under the same ET/H_2O, composite materials generated at different pyrolysis temperatures exhibited that as the BC ratio built up, the adsorption capacity increased first and then decreased (except for BC-nZVI prepared under the condition of an ET/H_2O ratio of 2 and pyrolysis temperature of 400°C). This was due to the agglomeration of an excess of nZVI particles when BC-nZVI was 1. When BC-nZVI was above 2, excessive BC blocked the active sites on the surface

of nZVI, and the presence of numerous pores made nZVI more distributed on the inner surface of BC, thereby reducing contact between nZVI and Se(IV). Two was an appropriate BC-nZVI, and Se(IV) removal capacity was optimal at this ratio. At different ET/H_2O, there was no distinct rule of Se(IV) adsorption. When a liquid-phase reduction method is used, as alcohol concentration increases, the particle size of nZVI is diminished [19]. Therefore, active sites of nZVI increased, and the Se(IV) removal capacity should build up. However, considering that excessive small particle size gave rise to agglomerate, the removal capacity would reduce instead, thereby bringing about unclear experimental rules. Under optimum BC-nZVI and pyrolysis conditions, the adsorption capacity reached the maximum when ET/H_2O was 1. Therefore, a BC-nZVI of 2 and ET/H_2O of 1 were chosen as the optimal raw material ratio to conduct follow-up adsorption experiments.

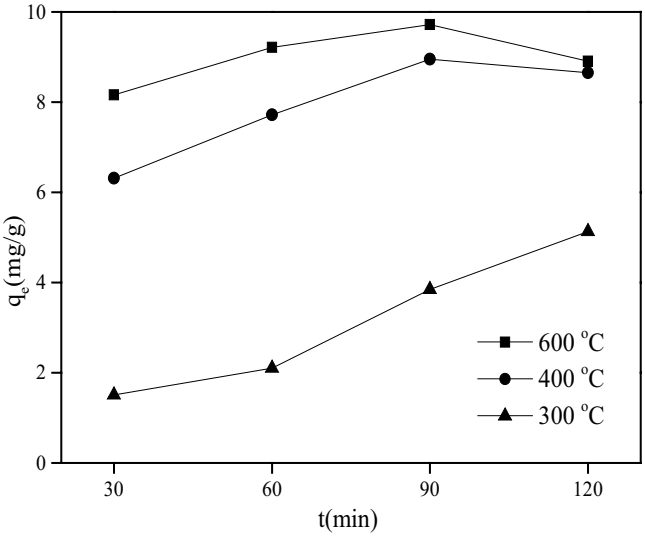

Fig. 1. The removal of Se(IV) by BC-nZVI prepared under different pyrolysis conditions (BC-nZVI and ET/H_2O were selected as 2 and 1, respectively).

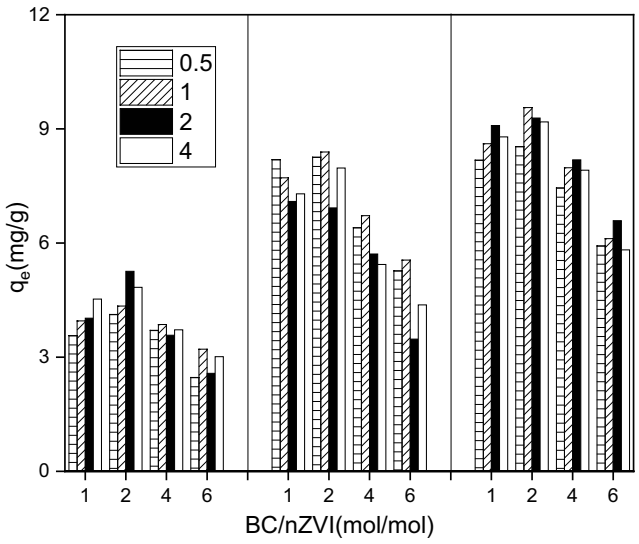

Fig. 2. The removal of Se(IV) by BC-nZVI prepared under different BC-nZVI and ET/H_2O.

To improve the performance of composite materials to remove Se(IV) under non-optimal pyrolysis conditions, BC prepared at 600°C and 30 min was selected to investigate the influence of chemical modification using diverse methods. As shown in Fig. 3, when BC_{600}-nZVI rose to 6, the adsorption capacity decreased markedly, which was due to the minimum adsorption capacity of BC_{600}-nZVI at this ratio. Three chemical modification methods were used by HCl, NaOH and H_2O_2 on the BC prepared at 600°C and 30 min, and these had different effects on the removal of Se(IV). The impact of HCl modification was not apparent, the modification of NaOH played a visibly stimulative role, and the modification of H_2O_2 showed the opposite effect. Dong et al. [7] found that negative charges on the BC surface had strong repulsive interactions with Cr(VI), so its removal capacity was negligible. As Se(IV) and Cr(VI) are both inorganic anionic pollutants, it was speculated that BC had no direct effect on the removal of Se(IV). Alkali-treated BC had a very high surface area [20], and as the support of nZVI, a larger surface area of BC can ensure that nZVI was evenly distributed, enhancing the possibility of contact with Se(IV). The larger surface area provides more places for the precipitate generated by the reaction, avoiding a decrease of nZVI active sites, thereby facilitating redox reactions. Hence, NaOH alkali modification enhanced the Se(IV) adsorption of BC-nZVI.

3.2. Surface functional groups

Fig. 4 presents the Fourier-transform infrared spectroscopy (FTIR) of diverse adsorbents. There were only a few weak peaks in BC, corresponding to a small number of functional groups. The band at 1,212 cm^{-1} indicated the presence of C–O, and its vibration at high temperature

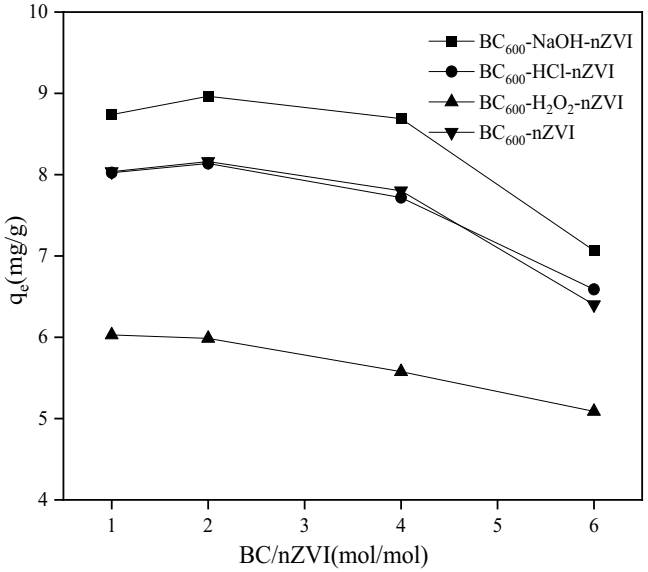

Fig. 3. The removal of Se(IV) by BC_{600}-nZVI prepared under different chemical modification.

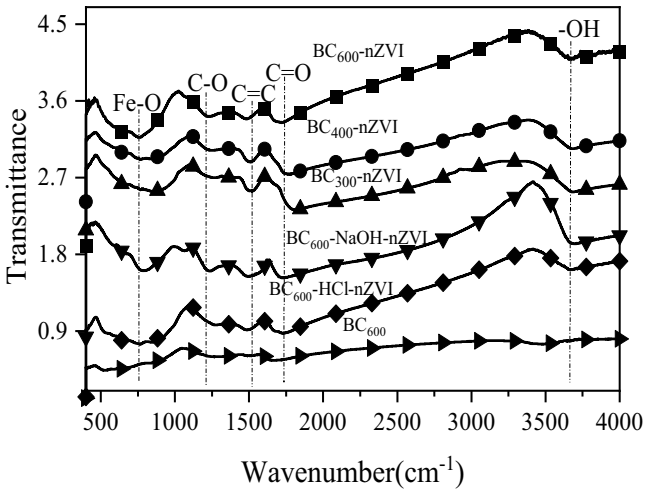

Fig. 4. Fourier-transform infrared spectroscopy of six materials.

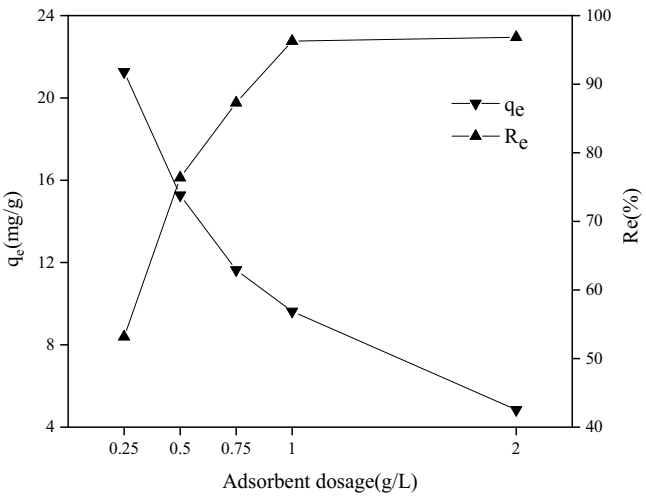

Fig. 5. The removal of Se(IV) by BC_{600}-nZVI at different dosages.

was enhanced. The band at 1,522 cm^{-1} was caused by aromatic C=C. With the increase of pyrolysis temperature, the intensity reduced, which was the consequence of decreased aromatization. The band at 1,734 cm^{-1} was related to C=O stretching, which was due to hemicellulose [21]. Compared with 300°C and 400°C, the weakening and decomposition of C=O appeared at a higher pyrolysis temperature (600°C). In addition, diverse chemical modifications also had a great influence on the surface functional groups. The band at 3,664 cm^{-1} arose from –OH. The vibration of –OH was weaker when modified by HCl, and was prominently enhanced when modified by NaOH, which was the largest infrared spectrum peak. Combined with the adsorption experimental data in Fig. 3, the –OH intensity made a great difference in the adsorption of Se(IV) [22]. A new absorption peak came out near 756 cm^{-1}, and it may be connected to the stretching of Fe–O, which indicated the successful loading of nZVI and slight oxidation on its surface.

3.3. Effect of adsorption conditions on the removal of Se(IV)

The effect of adsorbent dosage on the adsorption of Se(IV) is shown in Fig. 5. With the increase of adsorbent dosage, the adsorption capacity of BC_{600}-nZVI per unit mass diminished little by little, and the removal rate of Se(IV) grew to 96.84%, which was almost entirely removed. When adsorbent dosage was low, it was completely dispersed in the solution, and surface active sites were saturated, bringing about a high adsorption capacity of BC_{600}-nZVI. While small adsorbent dosage restricted the enlargement of the removal rate of Se(IV), when adsorbent dosage increased, the accumulation of BC_{600}-nZVI gave rise to incomplete exposure of the active site, so the adsorption capacity of BC_{600}-nZVI per unit mass decreased. Nevertheless, due to a good deal of BC_{600}-nZVI, the total number of active sites grew, and while the removal rate increased continuously, the growth trend gradually slowed down. When the dosage of BC_{600}-nZVI was 1 g/L, the removal rate of Se(IV) reached up to 96.28%. Thus, 1 g/L was an ideal dosage.

Fig. 6 shows the effect of the initial solution pH on the adsorption of Se(IV). When the initial pH rose from 3 to 10,

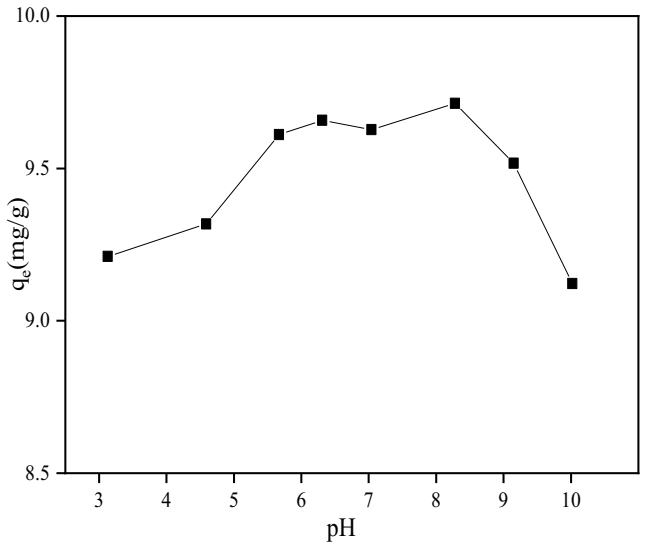

Fig. 6. The removal of Se(IV) by BC_{600}-nZVI at different initial solution pH.

the adsorption capacity of Se(IV) increased first and then decreased. The pH of solution exerted a notable influence on the reduction process of Se(IV). When pH was above 7, nZVI reacted: $Fe^0 + 2H_2O \rightarrow Fe^{2+} + 2OH^- + H_2$, in which the iron oxide generated by the reaction of OH^- with Fe^{2+} covered the surface of nZVI, preventing the electron transfer process between Se(IV) and nZVI [23]. Depending on previous studies, primary removal processes consisted of adsorption, reduction, and co-precipitation [24] was first adsorbed on the adsorbent surface, then Se^{4-} was reduced to Se^0 and Se^{2-} by electron transfer, and eventually reduction products co-precipitated with the corrosion products of nZVI. The reduction process was inhibited as alkalinity increased, and the adsorption capacity of Se(IV) gradually slowed down. Notably, in low pH, the adsorption capacity of Se(IV) was low, too [25]. This phenomenon differed from the conclusion that the adsorption capacity declined consistently

with the increase of pH [26], which may be due to taking into the role of straw biochar in adsorption account in this experiment. Although the largest adsorption capacity was attained at pH 8, the difference between pH 7 and pH 8 was small. A pH 7 was selected to be used in this experiment considering the economy and convenience.

3.4. Adsorption kinetics

The adsorption kinetics of different materials are shown in Fig. 7. The adsorption process was divided into three stages: rapid adsorption, slow adsorption, and adsorption equilibrium, respectively [27]. The fast adsorption in the early stage was due to the rapid occupation of surface active sites by Se(IV). And about 60 min later, the adsorption slowed down until it reached equilibrium. The kinetic model fitting parameters of six adsorbents are shown in Table 1. The pseudo-first-order model was based on physical adsorption, and the pseudo-second-order model assumed that the adsorption process was under the control of the chemical mechanism. Compared with the pseudo-second-order model (R^2 between 0.936 and 0.978), the pseudo-first-order model had a better fit (R^2 between 0.936 and 0.978), and the adsorption capacity predicted by it was also more close to the experimental value, indicating that in this experiment, the pseudo-first-order model was the optimal description for the removal of Se(IV). Therefore, the adsorption behavior of Se(IV) by BC_{600}-nZVI was determined by both physical and chemical mechanisms, of which physical adsorption dominated. Little difference between the pseudo-first-order rate constants of adsorption kinetics existed, demonstrating that equilibration time for diverse adsorbents was almost the same. The equilibrium adsorption capacity of BC approached 0, which verified the previous speculation that BC had no direct effect on the removal of Se(IV). Furthermore, the adsorption capacity of BC_{600}-NaOH-nZVI was greater than that of BC_S-nZVI, which prepared at 30 min, but less than that of BC_L-nZVI which prepared at 90 min. This made clear that NaOH modification can observably improve the removal performance of Se(IV) by BC_{600}-nZVI under non-optimal pyrolysis conditions, while the degree of promotion was limited.

In order to further explore the adsorption mechanism and learn about the rate-limiting steps of the adsorption process, the intraparticle diffusion model was utilized to fit the experimental data. The R^2 of six materials was between 0.764 and 0.864, and the fitting straight line didn't go through the origin, manifesting that intraparticle diffusion was not the only rate-limiting step.

4. Conclusions

BC-nZVI was prepared using a liquid-phase reduction method. Studies demonstrated that pyrolysis conditions

Table 1
Kinetic parameters of six materials

Adsorbent		Pseudo-first-order			Pseudo-second-order			Intraparticle diffusion		
	q_e [a]	q_e [b]	K_1	R^2	q_e [b]	K_2 (× 10^{-3})	R^2	K_p	C	R^2
BC	0.528	0.534	0.0380	0.991	0.665	56.8	0.975	0.0465	0.0688	0.864
BC_S-nZVI	8.38	8.48	0.0390	0.996	10.5	3.78	0.978	0.722	1.26	0.863
BC_L-nZVI	9.63	9.61	0.0440	0.994	11.7	4.03	0.973	0.775	1.99	0.834
BC_{600}-NaOH-nZVI	9.08	9.06	0.0420	0.963	11.1	3.88	0.963	0.758	1.58	0.829
BC_{600}-HCl-nZVI	8.21	8.23	0.0440	0.987	10.0	4.61	0.961	0.672	1.62	0.812
BC_{600}-H_2O_2-nZVI	5.83	5.79	0.0490	0.963	6.93	7.71	0.936	0.450	1.43	0.764

[a]Observed value.
[b]Calculated value.

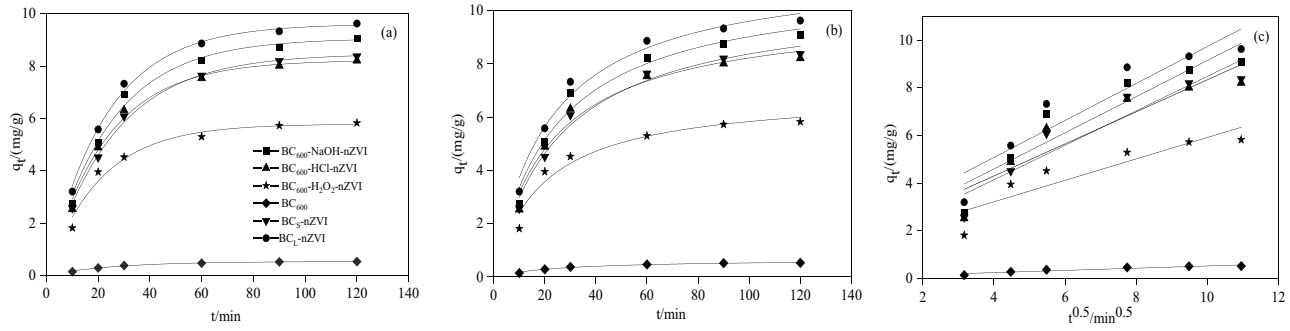

Fig. 7. Kinetics of adsorption of Se(IV) on diverse materials: (a) pseudo-first-order, (b) pseudo-second-order, and (c) intraparticle diffusion.

(BC-nZVI and ET/H_2O) markedly affected the removal of Se(IV). With the increase of pyrolysis temperature, the adsorption capacity of Se(IV) built up. At 300°C, as pyrolysis time rose, the adsorption capacity of Se(IV) gradually enlarged. Nevertheless, at 400°C and 600°C, the adsorption capacity increased first and then decreased. With the increase of the BC ratio, the adsorption capacity increased first and then decreased. Optimal preparation conditions were 600°C, 90 min, BC-nZVI of 2, and ET/H_2O of 1. NaOH modification enhanced the adsorption capacity of Se(IV), and when combined with FTIR data, it was observed that the –OH had a great influence on the adsorption of Se(IV). The consequences of batch adsorption experiments showed that with the increase of initial pH, the adsorption capacity by BC-nZVI increased first and then decreased. The adsorption of Se(IV) can fit the pseudo-first-order and pseudo-first-order models well, indicating that the adsorption behavior of Se(IV) by BC-nZVI was determined by both physical and chemical mechanisms, of which physical adsorption dominated. The fitting parameters of the intraparticle diffusion model manifested that intraparticle diffusion was not the only rate-limiting step.

Acknowledgments

This research was financially supported by the Enterprise Technology Innovation and Development Projects of Hubei Provincial (2021BAB115), the Key Research and Development Program of Hubei Provincial(2021BBA226), and the Foundation of State Key Laboratory of Coal Combustion (FSKLCCA2106). The authors also acknowledge the extended help from the Analytical and Testing Center of Huazhong Agricultural University (HZAU).

Declaration of interest statement

The authors declare that they have no known competing financial interests or personal relationships that could have appeared to influence the work reported in this paper.

References

[1] L.H.E. Winkel, C. Annette Johnson, M. Lenz, T. Grundl, O.X. Leupin, M. Amini, L. Charlet, Environmental selenium research: from microscopic processes to global understanding, Environ. Sci. Technol., 46 (2012) 571–579.
[2] Y. Xie, H. Dong, G. Zeng, L. Zhang, Y. Cheng, K. Hou, Z. Jiang, C. Zhang, J. Deng, The comparison of Se(IV) and Se(VI) sequestration by nanoscale zero-valent iron in aqueous solutions: the roles of solution chemistry, J. Hazard. Mater., 338 (2017) 306–312.
[3] S. Wang, Y. Zhou, B. Gao, X. Wang, X. Yin, K. Feng, J. Wang, The sorptive and reductive capacities of biochar-supported nanoscaled zero-valent iron (nZVI) in relation to its crystallite size, Chemosphere, 186 (2017) 495–500.
[4] H.E. Feng, D. Zhao, Manipulating the size and dispersibility of zerovalent iron nanoparticles by use of carboxymethyl cellulose stabilizers, Environ. Sci. Technol., 41 (2007) 6216–6221.
[5] T. Phenrat, N. Saleh, K. Sirk, R.D. Tilton, G.V. Lowry, Aggregation and sedimentation of aqueous nanoscale zerovalent iron dispersions, Environ. Sci. Technol., 41 (2007) 284–290.
[6] L.F. Greenlee, J.D. Torrey, R.L. Amaro, J.M. Shaw, Kinetics of zero valent iron nanoparticle oxidation in oxygenated water, Environ. Sci. Technol., 46 (2012) 12913–12920.
[7] H. Dong, J. Deng, Y. Xie, C. Zhang, Z. Jiang, Y. Cheng, K. Hou, G. Zeng, Stabilization of nanoscale zero-valent iron (nZVI) with modified biochar for Cr(VI) removal from aqueous solution, J. Hazard. Mater., 332 (2017) 79–86.
[8] H. Zhu, Y. Jia, X. Wu, H. Wang, Removal of arsenic from water by supported nano zero-valent iron on activated carbon, J. Hazard. Mater., 172 (2009) 1591–1596.
[9] S. Wang, B. Gao, Y. Li, A.E. Creamer, F. He, Adsorptive removal of arsenate from aqueous solutions by biochar-supported zero-valent iron nanocomposite: batch and continuous flow tests, J. Hazard. Mater., 322 (2017) 172–181.
[10] H. Wu, W. Wei, C. Xu, Y. Meng, W. Bai, W. Yang, A. Lin, Polyethylene glycol-stabilized nano zero-valent iron supported by biochar for highly efficient removal of Cr(VI), Ecotoxicol. Environ. Saf., 188 (2020) 109902, doi: 10.1016/j.ecoenv.2019.109902.
[11] S. Li, F. Yang, J. Li, K. Cheng, Porous biochar-nanoscale zero-valent iron composites: synthesis, characterization and application for lead ion removal, Sci. Total Environ., 746 (2020) 141037, doi: 10.1016/j.scitotenv.2020.141037.
[12] G. Tan, Y. Mao, H. Wang, M. Junaid, N. Xu, Comparison of biochar- and activated carbon-supported zerovalent iron for the removal of Se(IV) and Se(VI): influence of pH, ionic strength, and natural organic matter, Environ. Sci. Pollut. Res., 26 (2019) 21609–21618.
[13] X. Ling, J. Li, W. Zhu, Y. Zhu, X. Sun, J. Shen, W. Han, L. Wang, Synthesis of nanoscale zero-valent iron/ordered mesoporous carbon for adsorption and synergistic reduction of nitrobenzene, Chemosphere, 87 (2012) 655–660.
[14] Z. Saadati, M. Gilani, Kinetics, isotherms, and thermodynamic modeling of liquid-phase adsorption of Rhodamine B dye onto Fe/ZnO-shrimp shell nanocomposite, Desal. Water Treat., 85 (2017) 175–183.
[15] Y. Zhu, B. Yi, Z. Zong, X. Yang, M. Chen, Q. Yuan, Adsorption characteristic of organic matter by low-temperature dry cattle manure-derived anaerobic digestion, Desal. Water Treat., 225 (2021) 76–85.
[16] M. Ahmad, S.S. Lee, X. Dou, D. Mohan, J.-K. Sung, J.E. Yang, Y.S. Ok, Effects of pyrolysis temperature on soybean stover- and peanut shell-derived biochar properties and TCE adsorption in water, Bioresour. Technol., 118 (2012) 536–544.
[17] B. Zhang, J. Zhang, Z. Zhong, W. Wang, M. Zhu, Syngas production and trace element emissions from microwave-assisted chemical looping gasification of heavy metal hyperaccumulators, Sci. Total Environ., 659 (2019) 612–620.
[18] Z. Wang, K. Liu, L. Xie, H. Zhu, Y. Zhang, Effects of residence time on characteristics of biochars prepared via co-pyrolysis of sewage sludge and cotton stalks, J. Anal. Appl. Pyrolysis, 142 (2019) 104659, doi: 10.1016/j.jaap.2019.104659.
[19] Y. Chen, K.Y. Liew, J. Li, Size controlled synthesis of Co nanoparticles by combination of organic solvent and surfactant, Appl. Surf. Sci., 255 (2009) 4039–4044.
[20] H.M. Jang, S. Yoo, Y.-K. Choi, S. Park, E. Kan, Adsorption isotherm, kinetic modeling and mechanism of tetracycline on *Pinus taeda*-derived activated biochar, Bioresour. Technol., 259 (2018) 24–31.
[21] A. Kwarciak-Koziowska, R. Wlodarczyk, Efficiency assessment of coke industry wastewater treatment during advanced oxidation process with biochar adsorption, Desal. Water Treat., 199 (2020) 441–450.
[22] J. Song, S. Zhang, G. Li, Q. Du, F. Yang, Preparation of montmorillonite modified biochar with various temperatures and their mechanism for Zn ion removal, J. Hazard. Mater., 391 (2020) 121692, doi: 10.1016/j.jhazmat.2019.121692.
[23] H. Dong, Y. Chen, G. Sheng, J. Li, J. Cao, Z. Li, Y. Li, The roles of a pillared bentonite on enhancing Se(VI) removal by ZVI and the influence of co-existing solutes in groundwater, J. Hazard. Mater., 304 (2016) 306–312.
[24] B. Subramanyam, Liquid-phase adsorption of phenol onto blended adsorbents through bioremediation, Desal. Water Treat., 92 (2017) 181–195.
[25] C. Lei, B. Yi, W. Deng, M. Chen, Y. Wang, Effect of metal cationic on the adsorption of selenium from sewage by biochar

loaded with zero-valent iron, Desal. Water Treat., 245 (2022) 202–216.
[26] X. Xia, L. Ling, W.-X. Zhang, Solution and surface chemistry of the Se(IV)-Fe(0) reactions: effect of initial solution pH, Chemosphere, 168 (2017) 1597–1603.
[27] B. Wang, Y. Li, J. Zheng, Y. Hu, B. Hu, Efficient removal of U(VI) from aqueous solutions using the magnetic biochar derived from the biomass of a bloom-forming cyanobacterium (*Microcystis aeruginosa*), Chemosphere, 254 (2020) 126898, doi: 10.1016/j.chemosphere.2020.126898.